Geophysical Journal International

Geophys. J. Int. (2010) **182,** 421–432 doi: 10.1111/j.1365-246X.2010.04624.x

Seismic anisotropy of the Victoria Land region, Antarctica

S. Salimbeni, S. Pondrelli, S. Danesi and A. Morelli

Istituto Nazionale di Geofisica e Vulcanologia, Sezione di Bologna, Via D. Creti 12, 40128 *Bologna, Italy. E-mail: salimbeni@bo.ingv.it*

Accepted 2010 April 13. Received 2010 April 12; in original form 2009 December 1

SUMMARY

We present shear wave splitting results obtained from the analysis of core-refracted teleseismic phases recorded by permanent and temporary seismographic stations located in the Victoria Land region (Antarctica). We use an eigenvalue technique to isolate the rotated and shifted shear wave particle motion, to determine the best splitting parameters. Average values show clearly that dominant fast axis direction is NE–SW oriented, in accordance with previous measurements obtained around this zone. Only two stations, OHG and STAR, show different orientations, with N–S and NNW–SSE main directions. On the basis of the periodicity of single shear wave splitting measurements with respect to backazimuths of events under study, we infer the presence of lateral and vertical changes in the deep anisotropy direction. To test this hypothesis we model waveforms using a cross-convolution technique for the cases of one and two anisotropic layers. We obtain a significant improvement on the misfit in the double layer case for the two stations. For stations where a multilayer structure does not fit, we investigate lateral anisotropy changes at depth through Fresnel zone computation. We find that anisotropy beneath the Transantarctic Mountains (TAM) is considerably different from that beneath the Ross Sea. This feature influences the measurement distribution for the two permanent stations TNV and VNDA. Our results show a dominant NE–SW direction over the entire region, however other anisotropy directions are present and maybe interpreted in the context of regional tectonics.

Key words: Mantle processes; Seismic anisotropy; Antarctica.

INTRODUCTION

Splitting of shear waves from teleseismic earthquakes is a powerful tool to investigate the structure of the upper mantle in different geodynamic environments. Since anisotropy may be a result of deformational events, shear wave splitting studies permit investigation of the geodynamical processes, which have acted on the area of interest.

Shear wave splitting is the seismological analogue of optical birefringence. When an *S* wave passes through an anisotropic medium, it will be split into two quasi-*S* waves travelling with different velocities (Savage 1999). The vibration direction of the faster phase and the difference in arrival time (delay time) between the two phases, are parameters recovered from this analysis. Teleseismic shear wave splitting of core-refracted phases (e.g. SKS, SKKS) enables the study of the anisotropy located on the station-side of the epicentre-station path. Most of the anisotropy contribution originates in the upper-mantle region where olivine is the most abundant mineral (Silver 1996; Savage 1999). Since olivine is highly anisotropic, its crystals develop a preferred orientation when a geodynamical process acts. In the simple shear case, lattice-preferred orientation (LPO) is generated by dislocation glide (Karato *et al*. 2008) and (100) crystallographic axis rotates parallel to the direction of the maximum shear (Savage 1999) that also corresponds to the faster direction of *S*-wave vibration direction after splitting. Therefore the study of anisotropy can provide insights into deformational processes, which have acted at a regional scale.

The harsh climatic conditions and the inaccessibility of the Antarctic region make it difficult to operate permanent or long-term seismic instrumentation. Few data are available, therefore any additions to the collective data set are very important in understanding the tectonics of the Antarctic region. In recent years, several studies, which make use of seismic anisotropy, have been carried out, but the overall data set remains sparse. The current study adds new data and interpretation, which improves existing spatial coverage.

In East Antarctica (EA), previous shear wave splitting studies for the Dronning Maud Land area (Bayer *et al.* 2007) suggested mainly NE–SW anisotropy direction, with some nearly N–S directions, that authors interpreted as due to crust–mantle coupling deformation. NE–SW is also the main direction for stations located in other inland areas (e.g. at South Pole; Muller 2001), whereas shear wave splitting measurements for coastal stations are generally oriented parallel to the coastline as observed for the Lambert Glacier region (Reading & Heintz 2008). In West Antarctica (WA), NE–SW continues to be the dominant direction beneath the Transantarctic Mountain (TAM) belt (Barklage *et al.* 2009) and in the Victoria Land region (Pondrelli & Azzara 1998; Pondrelli *et al.* 2005). These measurements are interpreted to be related to the TAM uplift, whereas

NW–SE and E–W directions, present sporadically around the Ross Sea, are interpreted as linked to extensional processes, which have occurred in the past.

Some studies found also indications of possible two-layer anisotropic structure; Muller (2001) proposed the presence of two anisotropic layers beneath the Scotia Plate and beneath the western stations of Dronning Maud Land justifying the anisotropy sampled in the upper layer as due to the signature of an Archaean frozen-in anisotropy whereas the origin of the lower layer would go back to the Gondwana rifting stages. In the Lambert Glacier and Wilkes Land areas, Reading & Heintz (2008) admitted the possible presence of a two-layer structure for coastal stations even if the small amount of data did not allow modelling the upper-mantle anisotropy with the detail obtained by Heintz & Kennet (2006) for the adjacent Australian plate.

In the following, we describe the anisotropy measured for the Victoria Land region, WA. Using together data recorded at permanent stations VNDA and TNV and data from temporary stations sited around the David Glacier, we show the indications for the presence of different local domains of anisotropy, with a possible double-layer anisotropic system with lateral changes, a configuration more complex than that previously shown for this region. Here we provide an improved study of the regional seismic anisotropy distribution, we identify new heterogeneities and we describe a more detailed Victoria Land structure.

GEOLOGICAL AND GEOPHYSICAL SETTINGS

Antarctica is commonly divided into two main geological domains, East and West, with very different structural and geophysical characteristics (Fig. 1). EA is classified as a Precambrian craton, the central part of the Palaeozoic Gondwana super-continent. WA is interpreted as the assembly of Meso–Cenozoic crustal blocks (Dalziel & Elliot 1982) or microplates with metamorphic and volcanic terranes (Anderson 1999). The Ross Sea and the West Antarctic Rift System (WARS) are part of WA and represent the extensional basins developed after Cretaceous and Cenozoic extensions (Behrendt 1999). Evidence of active alkaline volcanism is present with Mount Erebus and Mount Melbourne volcanoes (Fig. 1).

The TAMs range separates the East from the West region of the continent. The TAM is a 3500-km long and 200-km wide chain composed, together with the Victoria Land region, of Cambrian and younger rocks. It is considered an intracontinental mountain belt with lack of evidence of compression. Its origin is attributed

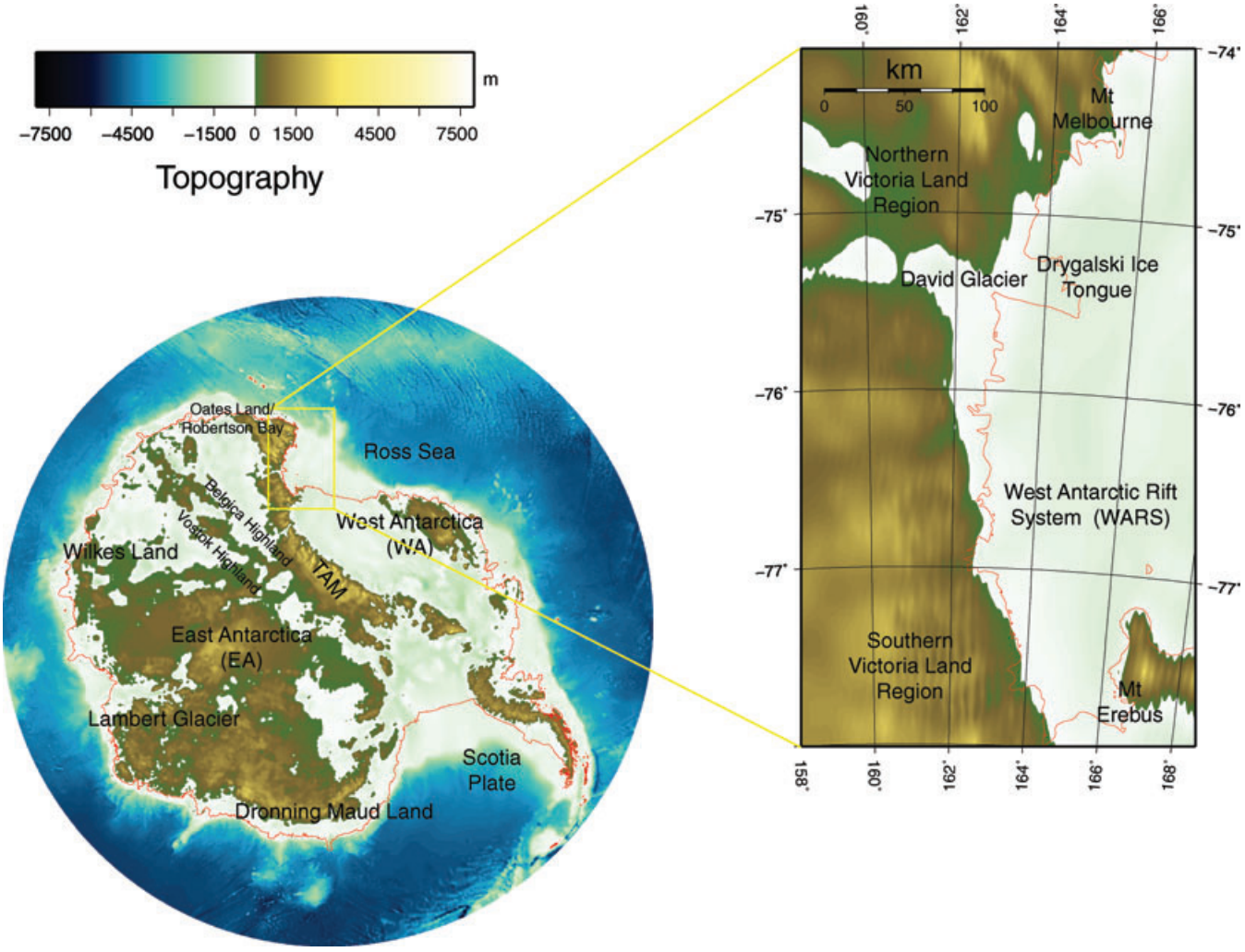

Figure 1. Map showing the elevation of the bedrock (Lythe *et al.* 2001) in Antarctica and main structural and seismic regions. The zoomed map corresponds to the Victoria Land region.

to an asymmetric uplift of the crust along the Ross embayment flank and subsequent denudation from Cretaceous to Cenozoic time (Fitzgerald 1992, 1995; Studinger *et al.* 2004). Fission track analyses (Fitzgerald 1992) establish the beginning of the main uplift phase at about 50 Ma.

Most of the surface and deeper geological structures of the Victoria Land region can be ascribed to the Ross Orogeny. The Meso–Cenozoic evolution of the Ross Sea has seen two main phases of extension; from 105 to 55 Ma, characterized by E–SE extensional faulting, and from 55 to 32 Ma, generating N–S and NNW–SSE tectonic depression. These extensional phases were followed by right-lateral strike-slip tectonics from 32 Ma to the present.

The tectonic fabric of the crystalline basement also originated during the Ross Orogeny, but in early Palaeozoic times (500–480 Ma). The fabric is defined by steeply dipping metamorphic foliation, highly strained shear zones and fold axial trends, in a main NW–SE direction (Salvini & Storti 1999). Surface structures in the Victoria Land region can be divided into three principal fault systems (Salvini & Storti 1999). The first one is a NW–SE right-hand strike-slip fault system along which major glaciers stream; the second one is composed by N–S depression profiles interpreted as extensional or transtensional structures associated to Cenozoic, right-lateral shear; the third one includes NE–SW and NNE–SSW faults present in the Terra Nova Bay area, bordering the western shoulder of the Ross Sea, connected to the TAM uplift. Fault directions are parallel to the coastline and tend to rotate to N–S and NW–SE moving towards south.

Several different seismological methods provide structural information, which highlights the dramatic discontinuity between East and West Antarctica.

Combining receiver function and phase velocity inversions, Lawrence *et al.* (2006b) derived crustal thickness in various parts of the study region. They show that beneath the Ross Sea the crust is 20 km thick (±2 km), and increases to 40 km (±2 km) beneath the TAM. A uniform 35-km thick crustal layer characterizes the cratonic domain in EA. These values are also in agreement with several previous works (Bentley 1991; ten Brink *et al.* 1997; Bannister *et al.* 2003). The crustal structure of northern Victoria Land has been investigated also by Piana Agostinetti *et al.* (2004). Analysing receiver functions they found a 24-km crustal thickness in the Robertson Bay area, with an increase to 31 km westward of the TAMs (Oates Land). This would suggest that the crustal profile remains approximately stable moving southwards beneath coastal stations, while it changes laterally (at different longitudes). Beneath the stations located in the TAM chain, the authors find evidence of two Moho interfaces between 26 and 48 km in depth.

Another seismological difference between East and West Antarctica concerns shear wave velocities. The TAM divides a 'fast' eastern upper mantle with velocities of 4.5 km s^{-1} (typical of a continental shield) from a 'slower' western one where velocities decrease to 4.2 km s^{-1} (typical for active tectonics and volcanic regions). These values are in agreement also with those inferred from the study of regional surface wave velocities (Danesi & Morelli 2001; Ritzwoller *et al.* 2001; Morelli & Danesi 2004). The transition between West and East occurs at 100 ± 50 km inland near the crest of the TAM (Lawrence *et al.* 2006c). The same transition separates a colder eastern region from a warmer western one (Lawrence *et al.* 2006a). The increment in mantle temperature is 200–400 °C (at 80–220 km depth), approximately corresponding to a reduction of 1 per cent in density.

Previous shear wave splitting measurements in the Victoria Land region and neighbouring areas are shown in Fig. 2. Pondrelli et al.

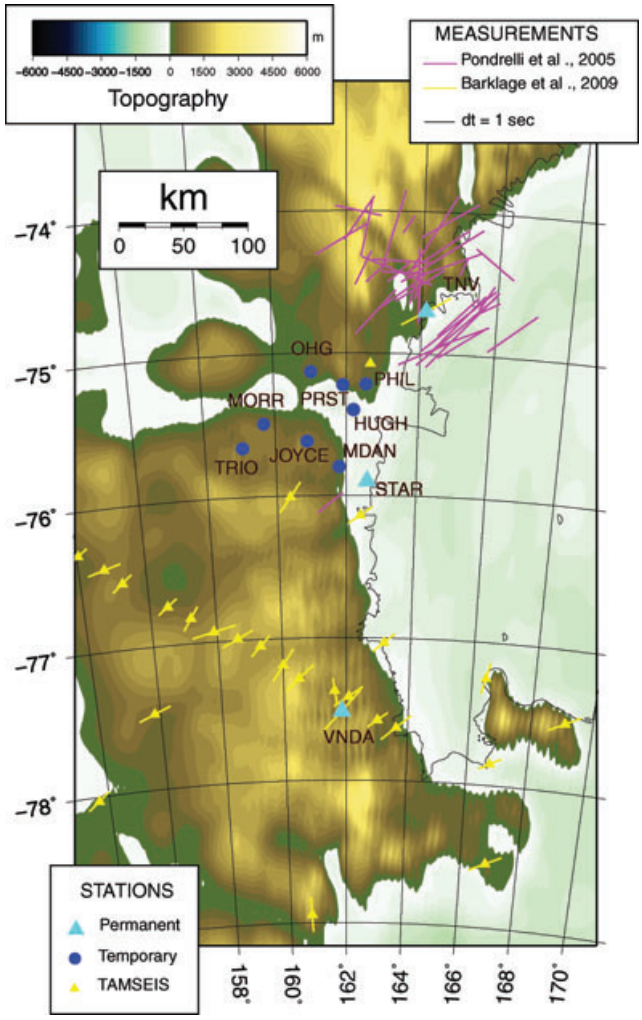

Figure 2. Map showing broad-band seismic stations operating in the Victoria Land region; cyan triangles are permanent stations (TNV, VNDA and STAR) and blue circles are temporary stations. Yellow triangles represent the TAMSEIS project stations. In the same map previous shear wave splitting measurements are shown; lines are oriented parallel to the fast axis with lengths proportional to delay time. Purple lines are results from Pondrelli *et al.* (2005) plotted for 150 km deep piercing points; yellow lines are results from Barklage *et al.* (2009) plotted at the surface.

(2005) measured shear wave splitting in the northern part of the study area (in purple in Fig. 2). Only non-null splitting measurements are plotted on the map and, following the representation of the authors, any measurement is plotted at location corresponding to 150 km of piercing point depth. This procedure is used only with measurements obtained from single-event analysis and each measurement is plotted at the surface projection of the ray path at the depth of 150 km. This representation evidences any difference in anisotropy as a function of backazimuth of studied events, to focus on the possible presence of lateral and vertical changes. The depth choice allows to interpret the total contribution of the anisotropy as located on the upper mantle (Savage 1999). Near TNV station, measurements have NE–SW dominant fast velocity direction while the average delay time is estimated around 1.6 s. The authors linked this NE–SW direction to the presence of an old cratonic anisotropy and to mantle flows due to the growth of the TAM chain. The other directions (E–W and NW–SE) instead are interpreted as due to the extensional processes associated with the Western Rift system.

Results from the TAMSEIS Project (in yellow in Fig. 2) are taken from Barklage *et al.* (2009). They obtained shear wave splitting teleseismic measurements for three temporary arrays (yellow triangles) located principally on the southern part of the Victoria Land and extending inland towards EA. Splitting parameters are calculated using stacked waveforms. At the intersections between E–W and N–S arrays, the fast direction is 58° and becomes more E–W towards the coast (67°). The delay time is about 1 s. At the same intersection, comparing Rayleigh wave phase velocities from different azimuth values, Lawrence *et al.* (2006c) found a fast axis direction ranging between 55° and 85° with magnitude of 1.5–3.0 per cent of anisotropy. In this area, Barklage *et al.* (2009) suggest anisotropy associated with an upper-mantle flow related to Cenozoic Ross Sea extension or an edge-driven convection due to the sharp thermal change between West and East Antarctica. Towards the EA instead the measurements are distributed along a 60° (±10°) direction that rotates to 15–20° (becoming E–W) in two highlands locations (Belgica and Vostok). The main distribution is described as being due to a relict tectonic fabric whereas the E–W measurements are interpreted as due to different extensional events maybe associated with older tectonic processes.

STATIONS AND DATA

We used data recorded by 11 seismic stations belonging to permanent and temporary networks in the Victoria Land region (Fig. 2 and Table S1 in supplementary material). Permanent stations (cyan triangles in Fig. 2) TNV and VNDA are located respectively on northern and southern margins of the study region. Both stations are equipped with three-component broad-band sensors (Streckeisen STS-1 and Geoteck KS-54000 Borehole, respectively) with free access data availability managed by IRIS consortium (http://www.iris.edu). In the region also temporary stations have been installed. In the course of two expeditions within the Italian Scientific Project PNRA, during the 2003–2004 and 2005–2006 austral summers, we installed nine broad-band temporary seismic stations (blue circles in Fig. 2) all equipped with Trillium T40 sensors and powered by solar panels and batteries. All the stations were located around the David Glacier running from the coast to the TAM on both sides of the glacier and cutting the chain perpendicularly, covering an area of 100×150 km^2. One of these stations (STAR, cyan triangle) became permanent at the end of the first expedition and it continues operating.

We analysed records of teleseismic events occurring between 2003 and 2007, with M_w greater than 5.5 and epicentral distance between 85° and 120°. This distance range increases the likelihood of the presence and easy identification of the SKS arrival. These choices allow us to have a data set for the temporary stations varying from a minimum of 2 months of data (e.g. site MORR) to a maximum of 5 yr (site STAR). For both the permanent stations (VNDA and TNV) instead a two-year long data set is complete.

SINGLE SHEAR WAVE SPLITTING MEASUREMENTS

The fast axis orientation and the delay time between faster and slower phases are the two parameters provided by shear wave splitting analysis. Most methods start assuming the anisotropic medium composed by one single layer with horizontal symmetry axis.

The fast velocity direction (ϕ) corresponds to the direction along which strain aligns the minerals; the delay time (dt) allows to estimate the thickness of the anisotropic material. We retrieved these two parameters using the Silver & Chan (1991) method. This is based on a grid search over the possible splitting parameters that better remove the effects of anisotropy from the waveforms. In a general case, this can be done searching the most singular covariance matrix based on its eigenvalues λ_1 and λ_2. A special case is when the initial wave polarization is known, as for SKS and SKKS phases, and when the signal-to-noise level is low; in this case the splitting parameters can be recovered minimizing the energy on the transverse component.

We used the SPLITLab environment (Wustefeld *et al.* 2008), a Matlab graphical user interface (GUI) that enables the analysis of shear wave splitting for large volumes of data and a quick quality check on the results. In addition, SPLITLab provides a method to calculate simultaneously shear wave splitting parameters using the eigenvalue approach (EV), minimization of energy on the transverse component (SC, notation from Wustefeld *et al.* 2008) and rotation-correlation (RC) technique (Fukao 1984; Bowman & Ando 1987) that removes the effect of splitting, maximizing the cross-correlation coefficient between radial (Q) and transverse (T) components of the waveforms in the selected windows.

As the initial polarization of the wave is assumed to be radial, RC and SC methods are applicable to phases as SKS and SKKS; the EV method instead uses the backazimuth as initial wave polarization and therefore it is applicable only for *S* phases. Synthetic tests on the RC and SC methods (Wustefeld & Bokelmann 2007) demonstrate comparable results when the fast axis is far enough from the backazimuth direction but show very different behaviours when the backazimuth is close to the fast or slow direction (null directions). In this cases, the RC method deviates by 45° from the input fast axis, while the SC method yields scattered estimates around it. Therefore a comparison of results between these two methods distinguishes null measurements from the real splitting cases and allows us to assign a quality flag for any single measurement (Wustefeld & Bokelmann 2007).

More specifically, we define the following parameters:

$\Delta\Phi = \Phi_{SC} - \Phi_{RC}$ and
$\rho = dt_{RC}/dt_{SC}$.

and we pick 'true' splitting measurements only if the following conditions are satisfied simultaneously:

(1) $\rho > 0.7$,
(2) $|\Delta\Phi| < 22.5°$, and
(3) signal-to-noise ratio (SNR) on the transverse component greater than 3.

The measurement is flagged as 'good' when $\Delta\Phi < 8°$ and $0.8 < \rho < 1.1$, 'fair' when $\Delta\Phi < 15°$ and $0.7 < \rho < 1.2$ and 'poor' in all other cases.

We consider null a measurement when an *S* wave travelling through the medium has no splitting. This happens when the medium is isotropic or when the wave propagates along the so-called null direction, that is the direction for which the initial wave polarization is parallel to the fast or slow axis (Savage 1999). For SKS and SKKS cases, these directions coincide with the backazimuth of the selected event. As suggested by Wustefeld & Bokelmann (2007), we can consider a measurement null when $\Delta\Phi \sim n \times 45°$ (with n an integer) and small ρ; we consider 'good nulls' when $37° < \Delta\Phi < 53°$ and $0 < \rho < 0.2$, 'fair nulls' when $32° < \Delta\Phi < 58°$ and $0 < \rho < 0.3$ and 'poor nulls' in all other cases or when the SNR is lower than 3.

In the following we will consider only the SC measurements and we compare them with the results of the RC method for the quality assignment only.

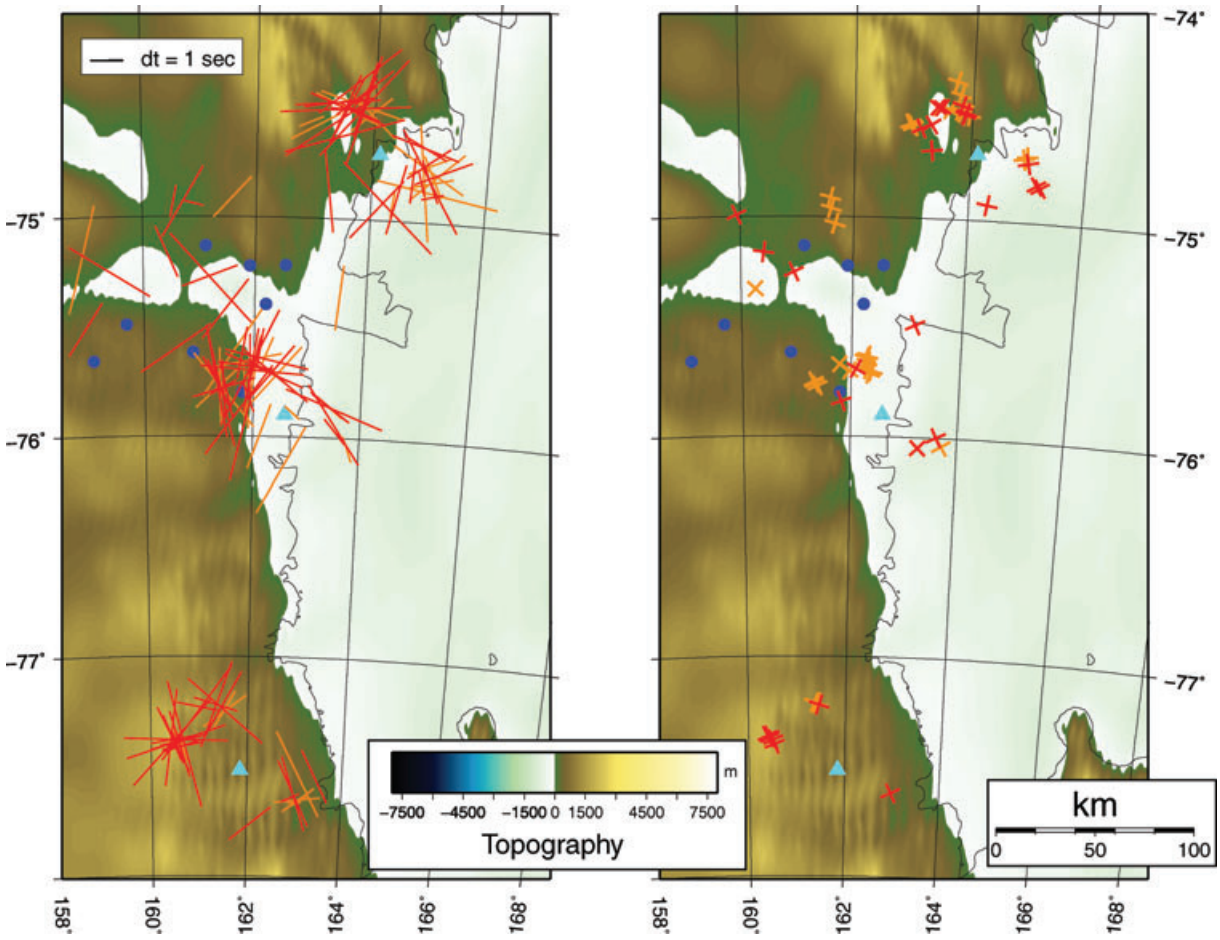

Figure 3. Single splitting (map on the left-hand side) and null (map on the right-hand side) measurements obtained using the method of Silver & Chan (1991). In both maps good (red) and fair (orange) measurements are plotted using a piercing point of 150 km. Splitting measurements are plotted with line-segment oriented parallel to the fast axis with lengths proportional to delay time; null measurements are plotted with two cross-line oriented parallel to the backazimuth and perpendicular to it. Blue circles and cyan triangles show locations (see Fig. 2 for colour legend).

Single station-event measurements obtained with the Silver & Chan (1991) method are shown on the map in Fig. 3 and listed in Table S2 (splitting measurements) and Table S3 (null measurements) of the supplementary materials. For the sake of simplicity, in red we have plotted measurements flagged as 'good' and in orange those flagged as 'fair'; all measurements are projected at a piercing point of 150 km depth to enhance any lateral variation in the anisotropy distribution beneath the station.

In total, we have 94 good and 44 fair splitting and 33 good and 37 fair null measurements. The distribution of the orientation of these measurements is very scattered (Fig. 3). NNE–SSW seems to be the most frequent fast direction, but also NNW–SSE or N–S measurements are well visible. For some stations we have measurements perpendicular to each other as an expression of the possible presence of a complex anisotropic structure beneath the region. Nulls measurement distribution is in agreement with this single-splitting pattern.

The distribution of average values of splitting measurements, were calculated for single stations (Fig. 4 and Table S4). When possible, the average values were calculated using good and fair measurements (dark blue segments) but in a few cases only fair measurements were used (cyan segments). In all cases nulls are excluded. Due to lack of results, caused by the few times of recordings and noisy data, in JYCE and MORR no average measurements are calculated. Most of the stations (TNV, VNDA, TRIO and HUGH) show a NE–SW direction and delay time values mostly compare well among them and in agreement with previous works. Station STAR has average fast axis with a NNW–SSE fast direction whereas in OHG the fast direction is N–S with a lower value of delay time. Stations with average anisotropy direction calculated with fair measurements (PHIL, PRST and MDAN) show a uniform NNE–SSW direction, quite different with respect to surrounding stations.

The distribution of the measurements directions is comparable with previous works (Pondrelli *et al.* 2005; Barklage *et al.* 2009). Our results however seem to estimate larger values of delay time; in fact, compared to the average values of 1 and 1.6 s calculated in the past, for most of our stations we also find values larger than 2 s and only at OHG we have a smaller delay time (1.5 s). This could be explained considering that we keep into account measurements until 4 s of delay time whereas the maximum value in Pondrelli *et al.* (2005) is 3 s providing smaller mean value. With respect to measurements in Barklage *et al.* (2009), instead, the difference is intrinsic in the calculation methods, given that in this last case the splitting parameters are calculated stacking waveforms for each station. In the next section, we will see that our mean values are comparable with those of this last work when we use a comparable method (as e.g. the cross-convolution technique).

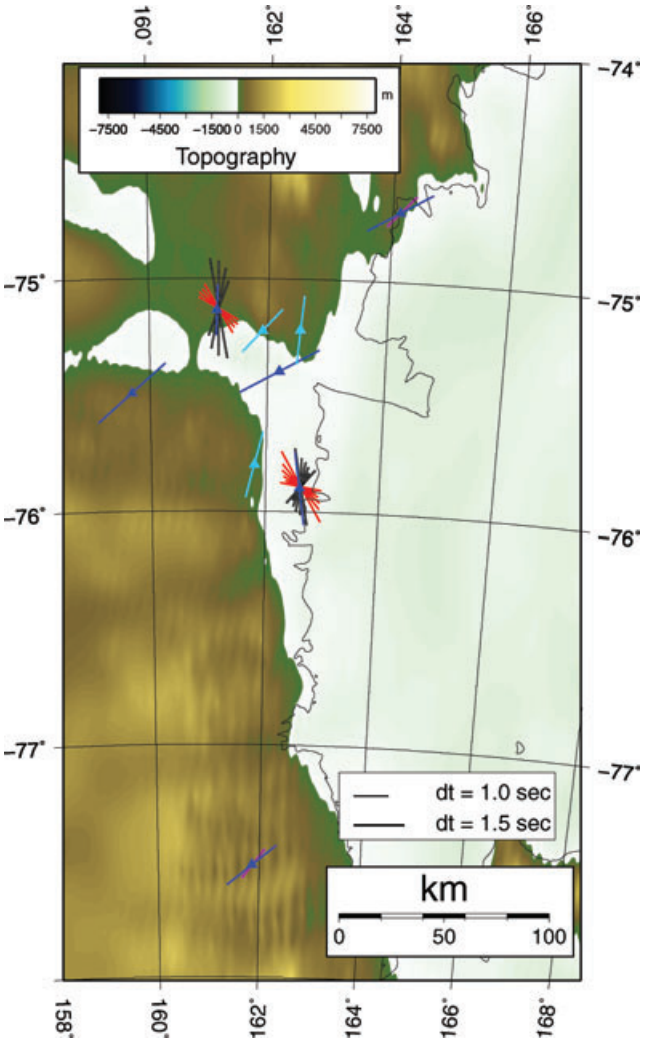

Figure 4. Average measurements (dark blue and cyan) and results of the inversion (violet and red-black lines) calculated for each station. Average measurements: results in blue are calculated using good and fair measurements whereas those in cyan are obtained with only fair measurements. Grouped inversion: for each station the 10 best solutions, with lowest misfit, are plotted. Violet lines represent one-layer best fitting model measures. Red and black lines respectively indicate lower and upper measures for two-layer best fitting models.

VERTICAL CHANGES OF THE ANISOTROPY

The SC and RC techniques described allow the calculation of the splitting parameters based on two main assumptions concerning the structure of the anisotropic medium to analyse. The anisotropic medium is supposed to have one single anisotropic layer with anisotropy oriented along its horizontal axis. The splitting parameters provide a true value if the earth structure is well drawn by the assumed model, whereas they give an 'apparent' result if the real earth structure beneath the study site includes two or more anisotropic layers or the symmetry axis is not horizontal. A periodicity of the splitting parameters pattern with respect to the backazimuth of the events usually indicates the presence of greater complexity (Savage 1999; Menke & Levin 2003).

To provide a possible interpretation to the variations that we obtain in our measurements, we studied the distribution of splitting parameters with respect to the backazimuth of teleseismic earthquakes. Examples for VNDA, STAR and TNV are shown in Fig. 5. Good (red crosses) and fair (blue crosses) splitting measurements and good (red circles) and fair (blue squares) null measures are displayed. The distribution of fast axis and delay time with respect to the backazimuth seems to fit with different types of two-layer models (represented by green lines). The distribution of earthquake's backazimuth is however discontinuous; for most events, phases under study come from NW or SE quadrants whereas the other backazimuths are absent. Therefore a unique interpretation would be unreliable.

To test the vertical variation of anisotropy in a different way, we use a cross-convolution technique (Menke & Levin 2003) to model all waveforms simultaneously and rebuild the complex pattern of our measurements; we try to fit the data with an adequate two-layer model.

The technique consists of two steps; first, splitting parameters for each event are calculated maximizing the cross correlation between horizontal rotated seismograms. Only events with a cross-correlation estimator value greater than 0.8 and modelled polarization within the error range of 20°, are picked for the following step. These criteria are so selective that only a small portion of data can be used for the inversion, generally about 8–9 per cent of the complete data set for each station. For this reason the inversion was carried out only for permanent stations TNV and VNDA and for those temporary stations having a wide range of day recordings, namely STAR and OHG. The final solutions have been obtained using a minimum of four (OHG) and a maximum of 24 (VNDA) events.

In the second step we find the unique earth model structure that satisfies the entire group of observations with a grid search inversion using a cross-convolution technique. Results are represented as an error surface plot as showed in Fig. 6. The more complex model is chosen considering the distribution of the models on error surface plots and on the misfit reduction. In the example, therefore, for TNV the one-layer model is chosen as the best fitting whereas the two-layer model seems to be the best for OHG. Where the best solution is a double layer model, the final solution is selected by excluding those with a delay time greater than or equal to 3.0 s and differences between two-layer fast axis orientations ranging between 80° and 100°. This choice avoids near-normal fast polarization values whereby delay time in one layer cancels the delay time in the other (Menke & Levin 2003).

The modelling results are displayed on the map in Fig. 4 and listed in Table S5 (supplementary material). Solutions for stations where a one-layer earth structure fits the waveforms better than a double layer model are shown with the violet lines oriented parallel to the fast axis and scaled accordingly to the delay time. Stations for which the double layer is the best model are represented with two colours: red for the lower and black for the upper layer. For each station the 10 solutions with lowest misfit are plotted.

Beneath VNDA and TNV stations, located, respectively on the southern and northern margin of the region, a vertical variation of the anisotropy is absent. From the inversion we deduced that beneath TNV the dominant anisotropy shows a fast direction between 41° and 44° and delay time between 1.1 and 1.2 s. For VNDA the situation is similar, with a fast direction between 36° and 39° and delay time ranging between 1.0 to 1.1 s. These values are consistent with the NE–SW alignment found for the averaged measurements and with previous papers.

Beneath STAR and OHG we infer that a two-layer structure provides a best fit to the available data. These sites are located on structurally different places: STAR is sited along the coast, in an area

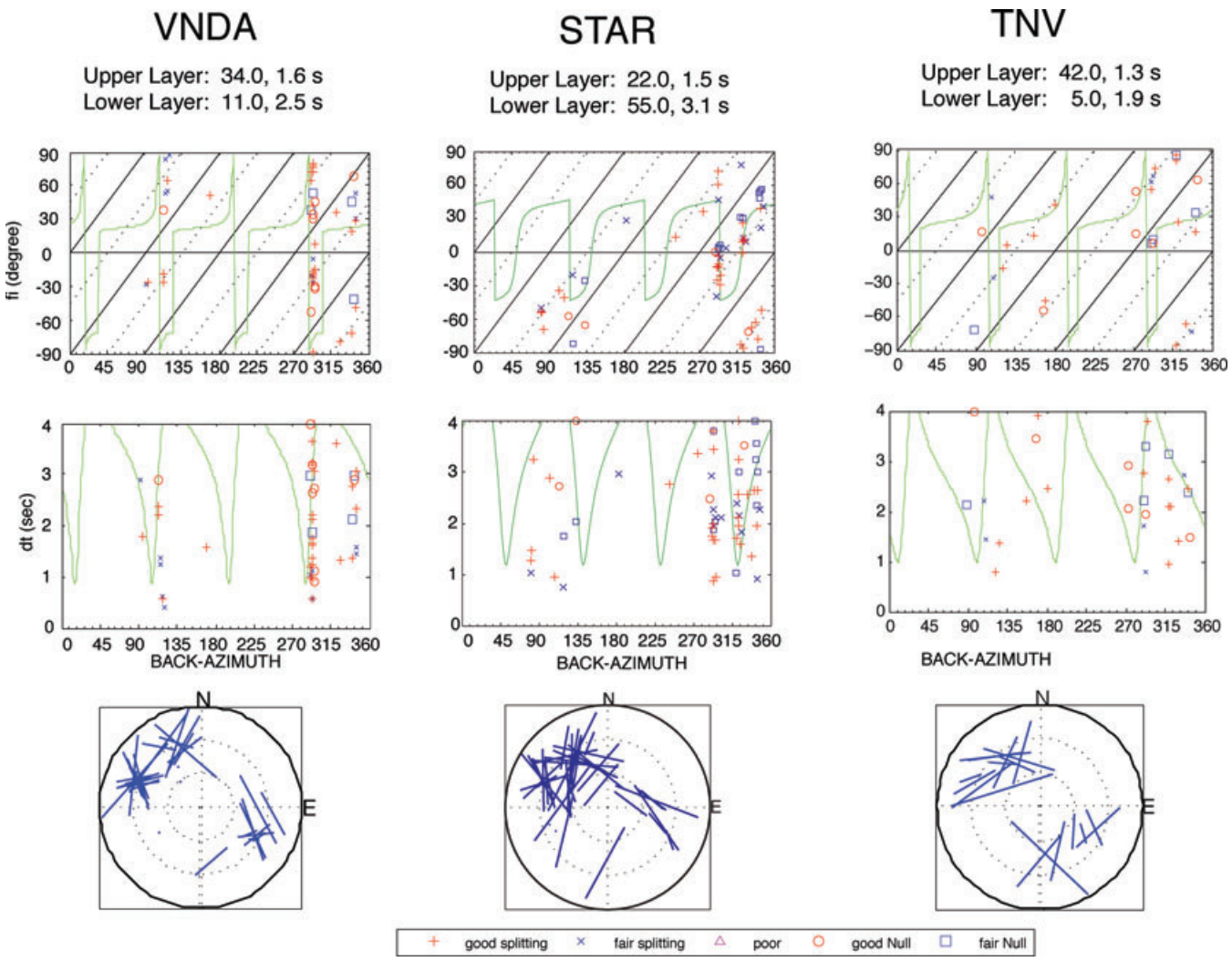

Figure 5. Examples of backazimuth dependence of the splitting parameters for VNDA, STAR and TNV stations. Each panel contains good (red crosses) and fair (blue crosses) split measurements and good (red circles) and fair (blue squares) nulls measurements. Poor results are excluded. Green lines in the upper and medium panels correspond to the theoretical distribution of two-layer model with splitting parameters described above each figure. The distribution of single measurements is showed on the lower plots.

where magma injection intruded along the Cenozoic N–S trending master faults (Rossetti *et al.* 2000) whereas OHG is located inland, on the eastern shoulder of Prine Albert Mountains, characterized by pre-Cenozoic basements (Rossetti *et al.* 2000). Nevertheless, the anisotropy shows similar patterns. Underneath STAR the fast axis for the lower layer varies from 100° to 150° and delay time from 0.9 to 2.3 s; in the upper layer respective intervals are −10° to 40° and 0.9 to 2.2 s. Beneath OHG, the fast axis direction for the lower layer varies in the range from 120° to 150°, time delay from 1.2 to 1.6 s; for the upper layer fast axis directions are from −10° to 20° and time delay from 1.7 to 2.9 s. All these measurements are mutually consistent and close stations show similar fast axis orientation for the upper layers (black lines).

LATERAL CHANGES IN THE ANISOTROPY DIRECTION

Results obtained for the two permanent stations TNV and VNDA show scattering in the single event-station measurements, but absence of evidence for multilayer structure. We hence investigate on the hypothesis of lateral changes of the anisotropy direction at depth as a possible interpretation of our measurements.

The computation of Fresnel zones, such as suggested by Alsina & Snieder (1995), helps to identify the presence of different patterns of anisotropy sampled from rays coming to the same station from different backazimuths. Taking into account where the rays have a common path beneath the station it is possible to identify the depth interval at which this change occurs (Fig. 7).

The disturbance generated by an earthquake is influenced by physical properties of the Earth in the vicinity of the geometrical ray path between source and receiver. This ray path can be approximated as a tube, the diameter of which is the Fresnel zone. The size of the Fresnel zone is a function of the wave frequency, and distance along the ray. For a steep-incidence phase, such as SKS or SKKS, it is approximately proportional to the depth beneath the receiver. The Fresnel zone at the depth h, can be calculated using (Pearce & Mittleman 2002)

$$R_f = \frac{1}{2}\sqrt{Tvh},$$

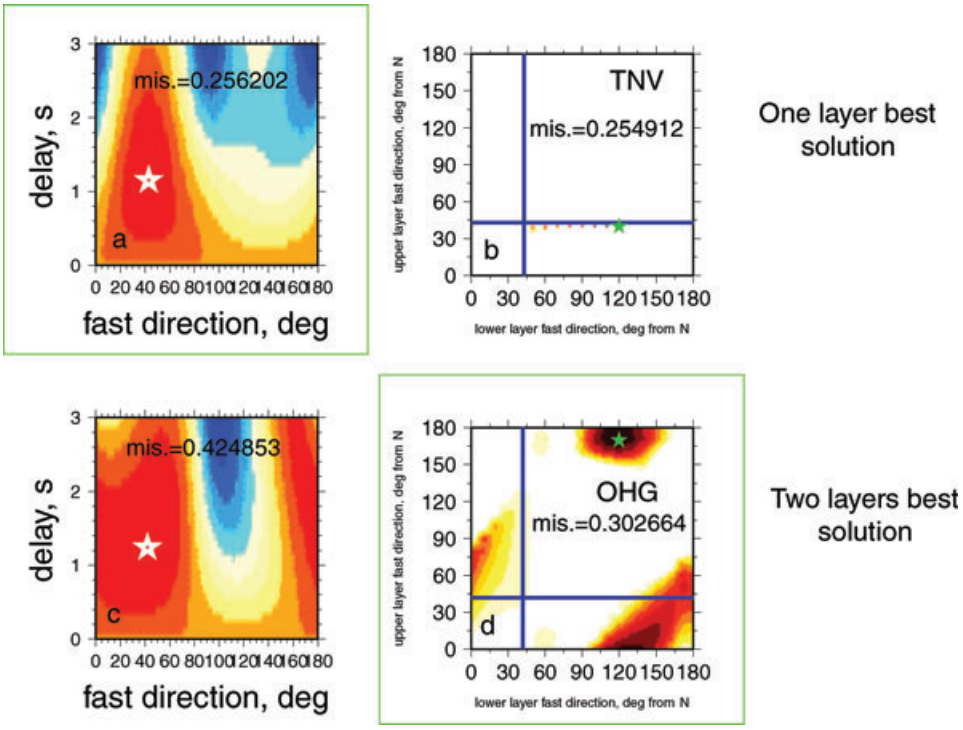

Figure 6. Examples of error surface plots calculated in the grouped inversion for TNV and OHG stations in one (a and c) and two layers (b and d) cases. (a) and (c) The white star indicates the minimum misfit error model. (b) and (d) In white all regions where errors are greater than the one layer estimator; coloured areas correspond to regions where errors are smaller for the two-layer case. The two blue crossing lines correspond to the one-layer model solution. Green star is the lowest error misfit model.

where R_f is the radius of the Fresnel zone expressed in km, T is the dominant period of the wave and v is the wave velocity. We choose $T = 10$ s as the dominant period of the wave, with the corresponding shear wave velocity of S phase obtained from IASP91 model (3.75 km s^{-1} at 35 km, 4.476 km s^{-1} at 50 km, 4.49 km s^{-1} at 100 km, 4.45 km s^{-1} at 150 km, 4.5 km s^{-1} at 200 km and 4.6 kms^{-1} at 250 km).

Examples for VNDA and TNV stations are shown in Fig. 7; for each station we mapped the shear wave splitting direction obtained studying two events coming from opposite backazimuths. The two rays visibly sample different anisotropic patterns. If we take into account that these two rays share the same path beneath the station (see sketch included in Fig. 7), the lateral change in the anisotropy should lay deeper than their conjunction point (Z depth on the inset). Indeed, below this depth the rays sample different regions of the upper mantle (blue circles in Fig. 7) and above this depth the rays travel through the same anisotropic medium (yellow circles). The Fresnel zones are calculated for 35, 50, 100, 150, 200 and 250 km of depth. Shared paths are represented by intersecting circles following opposite rays, vice versa paths along which rays are separated (thus, sampling different regions) are represented by non-crossing circles. The boundary between crossing and separated circles defines the depth at which the lateral variation occurs. We can deduce that for VNDA the lateral variation on the anisotropic properties occurs between 50 and 100 km of depth (last crossing and first separated circles, respectively) whereas beneath TNV it occurs between 100 and 150 km of depth.

When we analyse rays coming from NW at both permanent stations, we obtain similar results, which indicate a dominant NE–SW anisotropy direction beneath the TAM. This is the most frequently measured direction for the region with no dependency on the recovery method.

On the contrary, rays coming from east seem to sample different anisotropic structures at the two sites—WNW–ESE for TNV and NW–SE for VNDA. These observations indicate two distinct anisotropic characters in the TAM and the Ross Sea Embayment.

DISCUSSION

Fig. 8 summarizes all our shear wave splitting results (in colour) in the Victoria Land zone; for comparison we add measurements obtained by previous studies (in grey). The figure indicates the presence of different domains of anisotropy between margins and central part of the Victoria Land region.

At station TNV (northern region) we have a general agreement between different measurements. The NE–SW trend found by Pondrelli *et al.* (2005) and lately confirmed by Barklage *et al.* (2009) is in agreement with both our average of single measurements (blue stick) and our group inversion model (violet stick). Our last analysis suggests that the scattering in single measurements should not be ascribed to a vertical change in the anisotropy direction, at least at lithosphere–asthenosphere structure scale. The Fresnel zone computation shows that a lateral variation in anisotropic character at depth beneath TNV explains the splitting directions moving away from the dominant NE–SW.

In the southern region we have a similar situation. Our results for VNDA station are consistent and also agree with the splitting directions obtained for the temporary TAMSEIS network (in grey). The NE–SW direction is generally confirmed for stations moving towards the north. Again, the group inversion using our data excludes a vertical change in anisotropy directions beneath VNDA (at least at the scale we can investigate), whereas our Fresnel zone

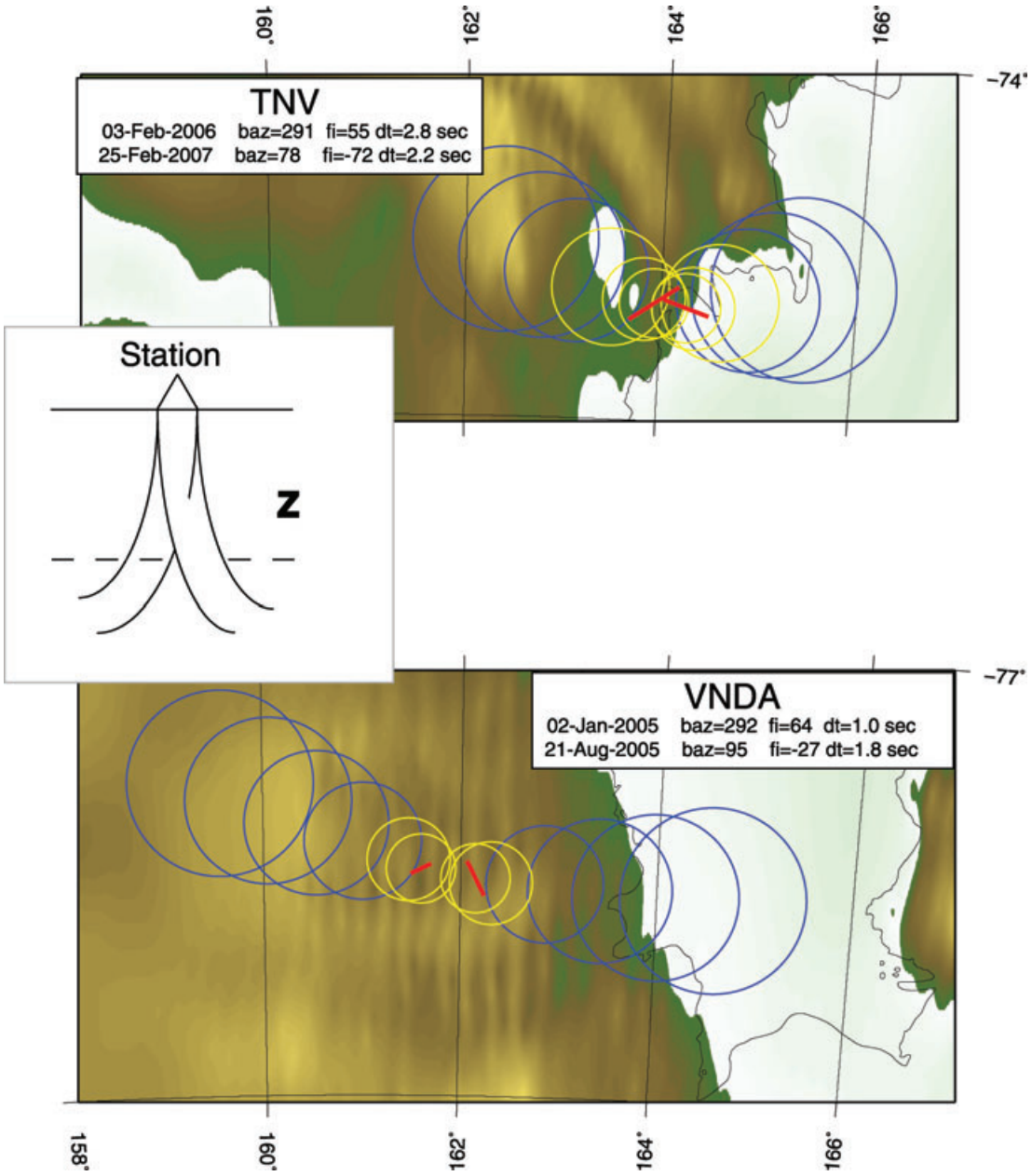

Figure 7. Examples of Fresnel zones analysis for TNV and VNDA. Two events with opposite backazimuth and different splitting parameters are analysed. Different size on the circles corresponds respectively to 35, 50, 100, 150, 200 and 250 km of depth of the Fresnel zone. In red we show the splitting measurements plotted at 35 km of depth. All intersecting circles in yellow represent the depth (*Z* on the inset) above which rays sampled the same anisotropy; in blue, separated circles define the depth below which rays sampled mediums with different anisotropic properties.

analysis supports the possibility of a lateral change at depth. This allows us to explain the single measurements trending away from the main NE–SW direction.

Some estimates for the thickness of the anisotropic layer in the area can be inferred from delay time values of the grouped inversions. In both North and South Victoria Land, delay times range between 1.0 and 1.2 s. Given that Lawrence *et al.* (2006c) estimate 1 s delay time for a 150-km thick anisotropic medium, with 3 per cent anisotropy, we infer that the thickness of the anisotropic layer should vary between 150 and 180 km.

From the calculation of the Fresnel zone, we can affirm that the anisotropic material should lay at a depth larger than 50–100 km (smaller values obtained, respectively for VNDA and TNV), therefore the anisotropy thickness become in general greater than 200 km in depth. Since the lithosphere thickness beneath the Ross embayment was calculated in 250 km (Morelli & Danesi 2004), anisotropy would be partially located in the lower lithosphere, with a possible contribution to the asthenospheric mantle.

The central part of the region has different features. The first difference is the direction of average fast axis measurements in OHG and STAR, which are N–S and NNW–SSE, respectively. The mean directions calculated using only fair measurements (light blue stick in Fig. 8) follow the same pattern.

Group inversion here gives a two-layer anisotropic model with NW–SE direction for the lower layer and N–S for the upper one. Since OHG is located on thick crust (about 35 km; Lawrence *et al.*

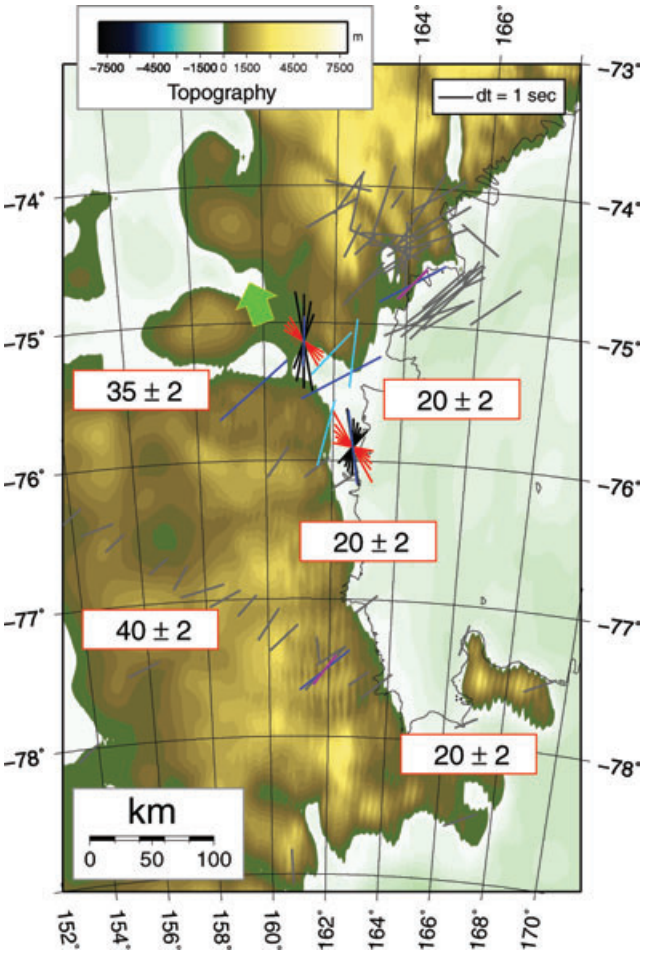

Figure 8. Summary map of shear wave splitting results. Mean values of the single shear wave splitting, calculated using good and fair split measurements, are in dark blue; mean values calculated with only fair measurements are in light blue; results from group inversion where the best model is the single one (10 better solutions) are in violet; red and black are 10 better solutions for lower and upper layer, respectively. Previous results of Pondrelli *et al.* (2005) and Barklage *et al.* (2009) are plotted in grey. The big green arrow indicates the absolute plate motion of the Antarctica plate (Gripp & Gordon 2002). Crustal thickness is taken from Lawrence *et al.* (2006b).

2006c) and STAR on thinner crust (about 20 km), and considering that the anisotropy direction shows the same pattern, it is reasonable to expect that the anisotropy distribution is independent from the shallower structure, excluding (or limiting) a possible crustal contribution. Delay time values vary between 1.2–1.6 and 0.9–2.3 s in the lower layers and between 1.7–2.9 and 0.9–2.2 s in upper ones for OHG and STAR, respectively, providing estimates for anisotropy thickness of 435–675 km beneath OHG and 270–675 km beneath STAR. Considering that the lithosphere thickness is approximately 250 km, we infer an asthenospheric contribution.

From these results it appears that a narrow zone (approximately 100–150 km) separates a dominant NE–SW anisotropy of the northern and southern areas from the double layer structure inferred for stations closer to the David Glacier. Dominant directions for upper and lower layers are N–S and NW–SE, respectively. The first orientation is in agreement with results found at some stations of the TAMSEIS array (grey lines in Fig. 8) whereas the second direction matches with some single measurements close to station TNV (grey lines in Fig. 8; Pondrelli *et al.* 2005). TRIO and HUGH, temporary stations located in the central part of the study region, have a NE–SW mean value. On these sites, however, we could not apply group inversion or the Fresnel zone technique for lack of usable data.

Our measurements of anisotropy can be easily related to the tectonic features in the area, which indicate that crust and subcontinental mantle deform coherently (vertically coherent deformation, VCD, as defined by Silver 1996). The basic idea is that when more than one deformational event occurs, the effect of the younger is recorded on the hotter and deeper layer, whereas the oldest event remains recorded in the shallower and colder layer. With this concept in mind, we interpret the double layer anisotropic structure: the N–S direction of shallow anisotropy would be related to the deformation occurred during the second phase of extension (55–32 Ma), and the lower layer anisotropy would be related to the last transtensional event, that is still going on (32 Ma to the present). In this context the NE–SW anisotropy can be interpreted as frozen-in anisotropy relative to older geological events as inferred by several authors (Pondrelli *et al.* 2005; Barklage *et al.* 2009), overprinted locally by more recent tectonic events. This hypothesis would also agree with possible lateral variations at depth. In fact, the contribution from western paths is in agreement with the NE–SW frozen-in anisotropy that would be beneath the TAM chain. More recent tectonic events have been taking place mainly in the Ross Sea, beneath which we sample WNW–ESE to N–S anisotropy directions.

Our measurements could also indicate an absolute plate motion (APM) contribution. The APM for the Antarctic plate on the Victoria Land region is 18° from N (green arrow in Fig. 8; Gripp & Gordon 2002) that is quite similar to the lower layer anisotropy direction. We therefore could deduce that the frozen-in anisotropy existing in the upper layer is linked to the two extensional phases of the Ross Orogeny and the APM contribution is constrained to exist in the lower layers. This hypothesis has been already investigated by Kendall *et al.* (2002) studying seismic anisotropy in continental environments as the Canadian shield. However, the low velocity of the Antarctic plate (1.3–1.6 mm yr^{-1}) does not produce necessarily the strain needed to generate this amount of anisotropy. Therefore, in agreement with Barklage *et al.* (2009), we suggest that this mechanism is not likely to be significant in the region that has been investigated in this study.

CONCLUSIONS

Shear wave splitting measured in the Victoria Land region indicates that the NE–SW anisotropic direction is the most frequent orientation of anisotropy for stations located on northern and southern domains of the study region, in agreement with previous measurements. Here we add some new data supporting the presence of a lateral variation at depth, represented by a mainly NE–SW anisotropy direction beneath the TAM and some indications of a WNW–ESE to NW–SE anisotropy beneath the Ross Sea. For stations located around the David Glacier the distribution of single measurements is more scattered and the grouped inversion is consistent with the presence of a double anisotropic layer for the central area of the Victoria Land. The two dominant directions are N–S and NNW–SSE for the upper and lower layer, respectively, in agreement with the direction of most of the tectonic structures in the area, presumably generated during the Ross Orogeny deformational phases.

This work has provided improved insights into the regional seismic anisotropy pattern, including newly identified heterogeneities and a more detailed picture of the structure of Victoria Land.

Continued improvements to the database in the course of new field campaigns will allow further refinement of these results.

AKNOWLEDGMENTS

We are very grateful to the referees, Dr A.M. Reading and Prof J. Trampert, for their constructive comments, which contributed to improve the manuscript. This work is supported by Programma Nazionale di Ricerche in Antartide (PNRA). All figures have been produced using the GMT package (Wessel & Smith 1991, 1998).

REFERENCES

Alsina, D. & Snieder, R., 1995. Small-scale sublithospheric continental mantle deformation: constraints from SKS splitting observations, *Geophys. J. Int.,* **123,** 431–448.

Anderson, J.B., 1999. *Antarctic Marine Geology*, Cambridge University Press, Cambridge.

Bannister, S., Yu, J., Leitner, B. & Kennett, B.L.N., 2003. Variations in crustal structure across the transition from West to East Antarctica, Southern Victoria Land, *Geophys. J. Int.,* **155,** 870–884.

Barklage, M., Wiens, D.A., Nyblade, A. & Anandakrishnan, S., 2009. Upper mantle seismic anisotropy of South Victoria Land and the Ross Sea coast, Antarctica from SKS and SKKS splitting analysis, *Geophys. J. Int.,* **178,** 729–741.

Bayer, B., Muller, C., Eaton, D.W. & Jokat, W., 2007. Seismic anisotropy beneath dronning Maud land, Antarctica, revealed by shear wave splitting, *Geophys. J. Int.,* **171,** 339–351.

Behrendt, J.C., 1999. Crustal and lithospheric structure of the West Antarctic Rift System from geophysical investigations: a review, *Glob. Planet. Change,* **23,** 25–44.

Bentley, C.R., 1991. Configuration and structure of the subglacial crust, *in The Geology of Antarctica*, pp. 335–364, ed. Tingey, R.J., Oxford University Press, New York.

Bowman, J.R. & Ando, M., 1987. Shear-wave splitting in the upper-mantle wedge above the Tonga subduction zone, *Geophys. J. R. astr. Soc.,* **88,** 25–41.

Dalziel, I.W.D. & Elliot, D.H., 1982. West Antarctica: problem child of Gondwanaland, *Tectonics,* **1,** 3–19.

Danesi, S. & Morelli, A., 2001. Structure of the upper mantle under the Antarctic Plate from surface wave tomography, *Geophys. Res. Lett.,* **28,** 4395–4398.

Fitzgerald, P.G., 1992. The transantarctic mountains of Southern Victoria Land: the application of apatite fission-track analysis to a rift shoulder uplift, *Tectonics,* **11,** 634–662.

Fitzgerald, P.G., 1995. Cretaceous and cenozoic exhumation of the Transantarctic Mountains: evidence from the Kukri Hills of southern Victoria Land compared to fission track data from gneiss at DSDP site 270, *Paper presented at Seventh International Symposium on Antarctic Earth Sciences,* Terra Antarctic., Siena, Italy.

Fukao, Y., 1984. Evidence from core-reflected shear-waves for anisotropy in the earths mantle, *Nature,* **309,** 695–698.

Gripp, A.E. & Gordon, R.G., 2002. Young tracks of hotspots and current plate velocities, *Geophys. J. Int.,* **150,** 321–361.

Heintz, M. & Kennet, L.N., 2006, The apparently isotropic Australian upper mantle, *Geophys. Res. Lett.,* **33,** L15319, doi:10.1029/2006GL026401.

Karato, S., Jung, H., Katayama, I. & Skemer, P., 2008. Geodynamic significance of seismic anisotropy of the upper mantle: new insights from laboratory studies, *Ann. Rev. Earth planet. Sci.,* **36,** 59–95.

Kendall, J.M., Sol, S., Thomson, C.J., White, D.J., Asudeh, I., Snell, C.S. & Sutherland, F.H., 2002. Seismic heterogeneity and anisotropy in the western Superior Province, Canada: insights into the evolution of an Archaean craton, in *The Early Earth: Physical, Chemical and Biological Development*, pp. 27–44, eds Fowler, C.M.R., Ebinger, C.J. & Hawkesworth, C.J., Geological Society Special Publications, London, UK.

Lawrence, J.F., Wiens, D.A., Nyblade, A.A., Anandakrishnan, S., Shore, P.J. & Voigt, D., 2006a. Upper mantle thermal variations beneath the Transantarctic Mountains inferred from teleseismic *S*-wave attenuation, *Geophys. Res. Lett.,* **33**(3), L03303, doi:10.1029/2005GL024516.

Lawrence, J.F., Wiens, D.A., Nyblade, A.A., Anandakrishnan, S., Shore, P.J. & Voigt, D., 2006b. Crust and upper mantle structure of the Transantarctic Mountains and surrounding regions from receiver functions, surface waves, and gravity: implications for uplift models, *Geochem. Geophys. Geosyst.,* **7,** Q10011, doi:10.1029/2006GC001282.

Lawrence, J.F., Wiens, D.A., Nyblade, A.A., Anandakrishnan, S., Shore, P.J. & Voigt, D., 2006c. Rayleigh wave phase velocity analysis of the Ross Sea, Transantarctic Mountains, and East Antarctica from a temporary seismograph array, *J. geophys. Res.,* **111**(B6), B06302, doi:10.1029/2005JB003812.

Lythe, M.B., Vaughan, D.G. & Consortium, B., 2001. BEDMAP: a new ice thickness and subglacial topographic model of Antarctica, *J. geophys. Res.Solid Earth,* **106,** 11 335–11 351.

Menke, W. & Levin, V., 2003. The cross-convolution method for interpreting SKS splitting observations, with application to one and two-layer anisotropic earth models, *Geophys. J. Int.,* **154,** 379–392.

Morelli, A. & Danesi, S., 2004. Seismological imaging of the Antarctic continental lithosphere: a review, *Glob. planet. Change,* **42,** 155–165.

Muller, C., 2001. Upper mantle seismic anisotropy beneath Antarctica and the Scotia Sea region, *Geophys. J. Int.,* **147,** 105–122.

Pearce, J. & Mittleman, D., 2002. Defining the Fresnel zone for broadband radiation, *Phys. Rev. E,* **66**(5), 056602, doi:10.1103/PhysRevE.66.056602.

Piana Agostinetti, N., Amato, A., Cattaneo, M. & Di Bona, M., 2004. Crustal structure of northern Victoria Land from receiver function analysis, *Terra Antarctica,* **11,** 5–14.

Pondrelli, S. & Azzara, R., 1998. Upper mantle anisotropy in Victoria Land (Antarctica), *Pure appl. Geophys.,* **151,** 433–442.

Pondrelli, S., Margheriti, L. & Danesi, S., 2005. Seismic anisotropy beneath northern Victoria Land from SKS splitting analysis, in *Antarctica: Contributions to Global Earth Sciences*, pp. 153–160, eds Futterer, D.K., Damaske, D., Kleinschmidt, G., Miller, H. & Tessensohn, F., Springer-Verlag, Berlin Heidelberg, New York.

Reading, A.M. & Heintz, M., 2008. Seismic anisotropy of East Antarctica from shear-wave splitting: spatially varying contributions from lithospheric structural fabric and mantle flow? *Earth planet. Sci. Lett.,* **268,** 433–443.

Ritzwoller, M.H., Shapiro, N.M., Levshin, A.L. & Leahy G.M., 2001. Crustal and upper mantle structure beneath Antarctica and surrounding oceans, *J. geophys. Res.,* **106,** 30 645–30 670.

Rossetti, F., Storti F. & Salvini F., 2000. Cenozoic noncoaxial transtension along the western shoulder of the Ross Sea, Antarctica, and the emplacement of McMurdo dyke arrays, *Terra Nova* **12,** 60–66.

Salvini, F. & Storti, F., 1999. Cenozoic tectonic lineaments of the Terra Nova Bay region, Ross Embayment, Antarctica, *Glob. planet. Change,* **23,** 129–144.

Savage, M.K., 1999. Seismic anisotropy and mantle deformation: what have we learned from shear wave splitting? *Rev. Geophys.,* **37,** 65–106.

Silver, P.G., 1996. Seismic anisotropy beneath the continents: probing the depths of geology, *Ann. Rev. Earth planet. Sci.,* **24,** 385–432, doi:10.1146/annurev.earth.24.1.385.

Silver, P.G. & Chan, W.W., 1991. Shear-wave splitting and subcontinental mantle deformation, *J. geophys. Res. Solid Earth,* **96,** 16 429–16 454.

Studinger, M., Bell, R.E., Buck, W.R., Karner, G.D. & Blankenship, D.D., 2004. Sub-ice geology inland of the Transantarctic Mountains in light of new aerogeophysical data, *Earth planet. Sci. Lett.,* **220,** 391–408.

ten Brink, U.S., Hackney, R.I., Bannister, S., Stern, T.A. & Makovsky, Y., 1997. Uplift of the Transantarctic Mountains and the bedrock beneath the East Antarctic ice sheet, *J. geophys. Res.,* **102,** 27 603–27 621.

Wessel, P. & Smith, W.H.F., 1991. Free software helps map and display data, *EOS, Trans. Am. geophys. Un.,* **72,** 441.

Wessel, P. & Smith, W.H.F., 1998. New, improved version of generic mapping tools released, *EOS, Trans. Am. geophys.Un.,* **79,** 579.

Wustefeld, A. & Bokelmann, G., 2007. Null detection in shear-wave splitting measurements, *Bull. seism. Soc. Am.,* **97,** 1204–1211.

Wustefeld, A., Bokelmann, G., Zaroli, C. & Barruol, G., 2008. SplitLab: a shear-wave splitting environment in Matlab, *Comput. Geosci.-UK,* **34,** 515–528.

SUPPORTING INFORMATION

Additional Supporting Information may be found in the online version of this article:

Table S1. Coordinates of permanent and temporary stations operating in the Victoria Land region.

Table S2. Table of single measurements obtained with Silver & Chan (1991) technique.
Table S3. Table of null measurements obtained with Silver & Chan (1991) technique.
Table S4. Table of averaged single measurements.
Table S5. Results of grouped inversion.

Please note: Wiley-Blackwell are not responsible for the content or functionality of any supporting materials supplied by the authors. Any queries (other than missing material) should be directed to the corresponding author for the article.